Routes to fractality and entropy in Liesegang systems

Leen Kalash and Rabih Sultan

Citation: Chaos: An Interdisciplinary Journal of Nonlinear Science **24**, 023121 (2014); doi: 10.1063/1.4881077
View online: http://dx.doi.org/10.1063/1.4881077
View Table of Contents: http://scitation.aip.org/content/aip/journal/chaos/24/2?ver=pdfcov
Published by the AIP Publishing

Routes to fractality and entropy in Liesegang systems

Leen Kalash and Rabih Sultan[a)]
Department of Chemistry, American University of Beirut, Riad El Solh, 1107 2020 Beirut, Lebanon

(Received 11 February 2014; accepted 21 May 2014; published online 4 June 2014)

Liesegang bands are formed when solutions of co-precipitate ions interdiffuse in a 1D gel matrix. In a recent study [R. F. Sultan, Acta. Mech. Sin. **27**, 119 (2011)], Liesegang patterns have been characterized as fractal structures. In addition to experimentally obtained patterns, geometric Liesegang patterns were constructed in conformity with the well-known empirical laws. Both mathematical fractal dimensions and box count dimensions for images of PbF_2 and PbI_2 Liesegang patterns have been calculated. Liesegang patterns can also be described by the entropy state function, and categorized as more or less ordered structures. We revisit the relation between entropy and fractal dimension, and apply it to simulated geometrical Liesegang patterns. We have resort to three different routes for the estimation of the entropy of a Liesegang pattern. The HarFA software enabled the calculation of the Hausdorff dimension and the topological entropy, then the information dimension and the Shannon entropy. In a third pathway, analytical calculations were carried out by estimating the probability of occurrence of a fractal element or coverage. The product of Shannon entropy and Boltzmann constant yields the thermodynamic entropy. The values for PbF_2 and PbI_2 Liesegang patterns attained the order of magnitude of the reported Third Law entropies, but yet remained lower, in conformity with the more ordered Liesegang structures.
 [http://dx.doi.org/10.1063/1.4881077]

Liesegang patterns display bands of precipitate when interdiffusion of co-precipitate ions takes place in a gel medium. Because such stratification yields highly ordered structures, we are interested in calculating their entropy. We undertake such a task by relating entropy to the fractal dimension of experimentally and theoretically generated Liesegang patterns. Different methods used give consistent results, and the entropy approaches, but yet remains lower (as it should) than the Third Law entropy of the precipitate compound.

I. INTRODUCTION

Liesegang bands[2–4] are normally observed when two co-precipitate electrolytes interdiffuse in a gel medium, resulting in a spectacular scene of alternating precipitate and precipitate-free domains. The band formation is essentially attributed to a cycle of supersaturation, nucleation, and depletion—the so-called Ostwald cycle.[5,6] But a set of "post-nucleation" theoretical models constitutes another class of mechanisms, based on the Lifshitz-Slyozov[7] instability in a quasi-homogenously distributed sol of colloid precipitate particles. The present paper is concerned with an estimation of the absolute entropy of a Liesegang pattern with clear and distinct bands. To find a suitable approach and route to such a calculation, we resort to a possible relation between entropy and fractal dimension. In a recent study, Liesegang systems have been characterized as fractal structures.[1]

Fractal dimension and entropy were widely used in an inter-related context, and in a broad variety of applications, notably in geology, biology, and medicine. Entropy calculations were performed to characterize the global earthquake population, and the stability of the Earth system near criticality conditions.[8] The Earth mantle was described as an entropy sink[9] for dissipation from the system components of the surface plates, leading to a self-organized plate tectonics landscape. Statistical information entropy can be used to gauge the predictability of geomorphic reliefs.[10] Arzate-Vázquez *et al.*[11] developed the entropy/fractal dimension ratio for the evaluation of image complexity and roughness in a simultaneous way. They applied their method to the microstructure characterization of the texture of chitosan and alginate films.[11] In biology and medicine, the entropy function and fractal dimension are valuable tools in the analysis of heart and blood pressure rates,[12] EEG (electroencephalography) dynamics,[13] muscle ultrasound,[14] bone tissue regeneration,[15] and the perinatal model of human gravity transition.[16]

We carry out here a semi-empirical computation of entropy, with a focus on real PbF_2 and PbI_2 patterns prepared in the laboratory. The PbF_2 and PbI_2 Liesegang patterns had been classified as fractal chemical objects, and were characterized by a fractal dimension.[1] We also demonstrate an almost perfectly linear relation between entropy and fractal dimension.

Fractals are self-similar structures that replicate on different length scales. They are classified into natural fractals and geometrical fractals. Natural fractals[17] are those found in nature such as branching and ramifications in trees, while geometric fractals are those that could be assembled by successive subdivisions of a certain object according to rigorous mathematical rules.[18–21] Mathematical fractal geometry became a well-established characterization tool due to Benoît Mandelbrot,[19] known as the father of fractal theory, who also coined the term fractal. Whereas the geometric fractals display exact replications, the natural fractals are generally

[a)]Email: rsultan@aub.edu.lb

random. In Chemistry, macroscopic ramifications and dendritic shapes have been reported particularly in precipitate[22–24] and metal electrodeposition systems.[25,26] Even at the molecular level, fractal properties are manifested in the repeating distance of the unit cell in some metallic alloys,[27] and the structural replications in self-assembled macromolecules (dendrimers).[28]

A Liesegang pattern exhibits fractal ramification, in that a new forming band may be viewed as a ramified object from the preceding one. The 2D texture and morphology of the pattern consisting of the various band widths and band spacings in a repetitive rectangular framework, makes it approach a geometrical fractal like the Sierpinski carpet or the Cantor set.[19–21]

The purpose of this paper is twofold: 1. to add the Liesegang patterns to the class of systems where fractal dimension and entropy play a role in the characterization of the patterning features; 2. develop feasible methods of entropy calculation for Liesegang patterns through a variety of routes, to ensure a round and solid approach to the problem. This task frames Liesegang patterns into the set of applications, notably given the similarities between Liesegang banding and the banded scenery widely spread in geochemistry.

II. METHOD OF CALCULATION OF FRACTAL DIMENSION

We select two well-known Liesegang systems studied previously: PbF_2 and PbI_2.[29] The representative patterns are depicted in Fig. 1. The tubes are prepared with the following concentrations for PbF_2: $[Pb^{2+}]_0 = 0.250$ M, $[F^-]_0 = 0.045$ M; and for PbI_2: $[Pb^{2+}]_0 = 0.250$ M, $[I^-]_0 = 0.045$ M according to previously reported experimental procedures.[30] In both tubes, the lead ion Pb^{2+} lies in the outer electrolyte, and the anion (F^- or I^-) is in the inner. In such experiments, both electrolytes are doped in gel (agar).

A representative sample of 11 bands from each Liesegang pattern (PbF_2 and PbI_2) was photographed for

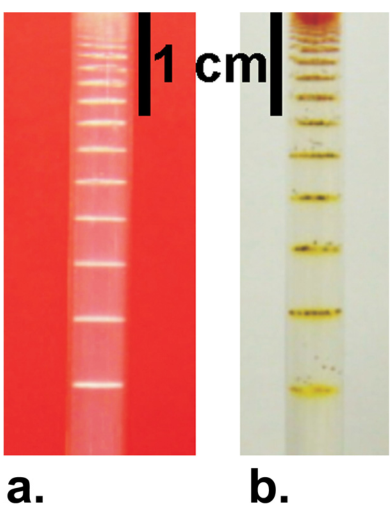

FIG. 1. Liesegang bands of white PbF_2 (frame a) and yellow PbI_2 (frame b). The concentrations used are: a For PbF_2 $[Pb^{2+}] = 0.250$ M (outer); $[F^-] = 0.045$ M (inner), both in 1% agar. b For PbI_2 $[Pb^{2+}] = 0.250$ M (outer); $[I^-] = 0.045$ M (inner), both in 1% agar.

fractal analysis. The images were transformed to black and white (BW) and the fractal dimensions were calculated by the box-count method. This necessitates the selection of a suitable threshold for the conversion. We decide on the threshold that gives the best visual BW contrast. We found that a variation of threshold over a 100 units range results in a standard deviation (SD) of 0.021 in the fractal dimension of the PbF_2 pattern. The reported value of 0.034 in Table I refers to the SD among the points (length scales) for a fixed threshold (yielding the best contrast). The SD value of 0.021 is across a wide range of chosen thresholds. Thus, we see that the image is robust and essentially insensitive to small threshold variations. The value of the fractal dimension ($D_{exp.}$) is primarily determined by the topology of the pattern. Simultaneously, we construct another set of BW pictures, but this time calculated from the well-known empirical laws.[31] These are the time,[32] spacing,[33] width,[34] and Matalon-Packter[29,35] laws. The band spacing of each Liesegang pattern (here PbF_2 and PbI_2) depends on the initial concentrations of the diffusing (outer) and immobile (inner) electrolytes ($[A]_0$ and $[B]_0$, respectively, which we will denote A_0 and B_0 for simplicity) in accordance with the Matalon-Packter law.[29] For those latter patterns constructed geometrically, both mathematically developed,[1] and box-count (on BW images) fractal dimensions were calculated.

The fractal dimension (D) is calculated for each pattern, using the box-count method. Since D is defined by the relation (1)

$$D = \frac{\ln[N(\lambda)]}{\ln[1/\lambda]}, \tag{1}$$

where λ is a length scale measuring unit, and $N(\lambda)$ is the number of squares covering the pattern, then D is obtained from the slope of the plot of ln $[N(\lambda)]$ versus $\ln[1/\lambda]$.

The calculation was performed by averaging over 20 length scales or square boxes of side λ, with $N(\lambda)$ designating the number of squares of side λ covering all the topological components of the pattern, as shown in Fig. 2 (the white bands).

The results are summarized in Table I ($D_{exp.}$). Because Liesegang bands are ordered structures that seemingly exhibit geometrical branching upon mathematical computation, the *analytical* method for calculating the fractal dimension is derived from geometrical patterns of strictly rectangular bands, generated as follows. By measuring band location (x_n) as a function of the concentrations A_0 and B_0, we can extract the mathematical expressions of the functions $F(B_0)$ and $G(B_0)$, which appear in the Matalon-Pactker law[29,31]

$$p = F(B_0) + \frac{G(B_0)}{A_0}, \tag{2}$$

TABLE I. Fractal dimensions of the PbF_2 and PbI_2 Liesegang patterns, obtained by various methods.

System	$D_{exp.}$	SD	$D_{anal.}$	$D_{geom.}$	$D_{Haus.}$
PbF_2	1.3676	0.0339	1.4003	1.3925	1.410
PbI_2	1.6331	0.0285	1.6334	1.6253	1.6129

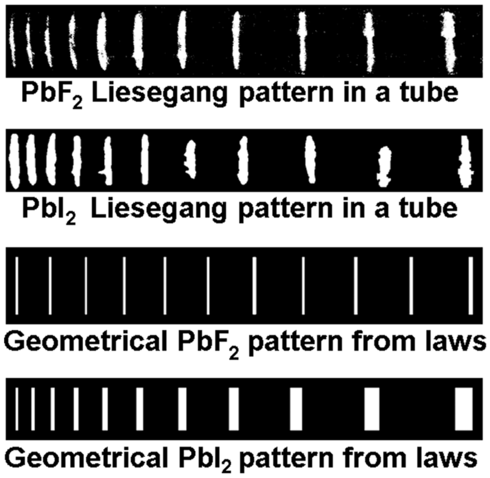

FIG. 2. Black and white pictures of Liesegang patterns of PbF_2 and PbI_2 for image analysis. Top two tubes: real experimental patterns. Bottom two tubes: geometrical patterns obtained by construction from the empirical laws. All patterns consist of 11 bands for consistency.

for each precipitate system independently.[29] Here p is the spacing coefficient, which appears in the spacing law[31,33]

$$\frac{x_n}{x_{n-1}} = 1 + p. \tag{3}$$

From the plots of the spacing coefficient p versus $1/A_0$ (Eq. (2)), we obtain, by curve fitting

For PbF_2:

$$F(B_0) = 10.4B_0^2 - 0.6773B_0 - 0.0397, \tag{4}$$

$$G(B_0) = -2.4444B_0^2 + 0.5633B_0 + 0.0082. \tag{5}$$

For PbI_2:

$$F(B_0) = 19.437B_0^2 - 4.8884B_0 + 0.2767, \tag{6}$$

$$G(B_0) = 0.66B_0 - 0.0004. \tag{7}$$

The location of band n (x_n) for each pattern is then calculated from Eq. (3). The width (w_n) of the n^{th} band is taken to obey: $w_n = mx_n^{\alpha}$ (with $m = 0.002$ and $\alpha = 1$) for PbF_2 and ($m = 0.017$; $\alpha = 1$) for PbI_2. The above calculation of x_n and w_n allows a full construction of the aforementioned geometrical patterns (Figure 2). The method for calculating the fractal dimension analytically for the geometrical pattern ($D_{anal.}$) is fully described in Ref. 1. The results are reported in Table I. In addition to this fractal dimension evaluation, we also calculate fractal dimension by the box-count method, but this time on the geometrical (not the experimental) patterns (called $D_{geom.}$, and recorded in Table I). We see that the D values are all essentially in good agreement.

III. ENTROPY

A. Rényi-Kolmogorov entropy

The PbF_2 and PbI_2 Liesegang patterns had thus been classified as fractal structures, characterized by a fractal dimension. Being categorized as ordered structures among an infinite family of fractal objects, it would be interesting to obtain an estimate of the absolute entropy of such patterns. As a first conceptual approach, the Rényi-Kolmogorov (R-K) entropy (S_q, often denoted K_q) describes the degree of chaoticity and diversity of a system, and gives the average rate of uncertainty or information loss about a position of the phase point on a given attractor.[36,37] The Rényi-Kolmogorov entropy of order q is defined for $q \geq 1$ (for $q \to 1$ as a limit) as

$$S_q(X) = \frac{1}{1-q} \ln \sum_{i=1}^{m} p_i^q, \tag{8}$$

where X is a discrete random variable, p_i is the probability of the event $\{X = x_i\}$. If the probabilities are identical, then all the Rényi entropies of the distribution become equal, and the equation of entropy becomes

$$S(X) = \ln m, \tag{9}$$

where m here is the event (or band) number. Generally, in a perfectly ordered system, $S_q = 0$ while in a totally random system $S_q \to \infty$, and in a chaotic system that is described by a state of deterministic chaos $0 < S_q < \infty$, where the parameter q refers to the entropy order. The R-K entropy (S_q) and generalized fractal dimension (D_q where the value of q is not specified) are connected by the linear relationship

$$S_q = D_q \ln r, \tag{10}$$

where r is the size of the X variable. The Shannon entropy S_1 in information theory is a special case of Rényi entropy where $q = 1$, and the thermodynamic entropy S is obtained upon multiplying the Shannon entropy by Boltzmann's constant k_B.[18]

Higher values of q that approach infinity result in a Rényi entropy that is greatly dependent on the highest probability events only, while lower values of q that approach zero give the Rényi entropy, which increasingly weights all possible events more equally, regardless of their probabilities. The case $q = 1$ represents an intermediate situation that characterizes the Shannon entropy with its unique properties; while when $q = 0$, the entropy is the logarithm of the size r of the support of X.[38]

B. Relation between entropy and fractal dimension

Various entropies of the fractal systems could be derived from the Rényi-Kolmogorov entropy of order q (Eq. (8)); also, a relation between the entropy and the fractal dimension could be derived. Lewis Fry Richardson[39] and Benoît Mandelbrot[19,40] studied the effect of changing the scale of measurement on the measured length. They showed that the coverage $n(\varepsilon)$ of an E-dimensional Euclidean space E by fractal structure, and the measured parts among the measured length of a border $N(\varepsilon)$ (Ref. 41) are connected by the relation

$$n(\varepsilon) = K\varepsilon^{E-D}, \quad N(\varepsilon) = n(\varepsilon)/\varepsilon^{E} = K\varepsilon^{-D}, \tag{11}$$

where ε is defined as the size measure and K is the number of measured parts for $\varepsilon = 1$. Mandelbrot[19] named the parameters

D and K as the fractal dimension and fractal measure for two and three-dimensional structures, respectively. The term $n(\varepsilon)$ is dependent on the size scale used for measurement, and the units depend on the dimension of the space E where the fractal structure is defined. The coverage $n(\varepsilon)$ represents either length of fractal structure (for $E=1$), its area (for $E=2$), or volume (for $E=3$).[41]

By comparing the equation of entropy (9) to the definition of fractal dimension (1) we get the following relation:

$$D = -\frac{d\ln N(\varepsilon)}{d\ln \varepsilon} \sim \frac{\ln m}{\ln r}. \tag{12}$$

As a consequence of Eq. (12), we get a linear dependence between the entropy and fractal dimension (Eq. (13)),[41] as follows:

$$S(r) = D\ln r. \tag{13}$$

C. Hausdorff dimension and topological entropy ($q=0$)

The topological entropy is the simple Rényi-Kolmogorov entropy defined for order $q=0$ (Eq. (14)); it does not depend on the probability (since $p_i^0=1$), but solely on the number of the events m with the probability $p_i>0$, where the events m are taken here as the bands themselves in our constructed geometric Liesegang pattern with location x_n, and with $\sum p_i = 1$. Recall that[18]

$$S_0(r) = \ln\sum p_i^0 = \ln m, \tag{14}$$

$$S_0(r) = D_0 \ln r. \tag{15}$$

The Hausdorff dimension D_0 is basically a description of the fractal geometry of the set that is characterized by its uniform density. It has been synonymously referred to as the capacity, box-counting dimension, or fractal dimension. Note that the last term is generic, and hence used for any dimension that may be nonintegral.[42] For most of the fractal sets of interest, the capacity and the Hausdorff dimension are equal.[42] It has been referred to as the capacity dimension since it provides information about how abundantly the measure is distributed over the scales of interest.[43] We use the HarFA 5.5 software (Harmonic and Fractal image Analyzer) to compute the Hausdorff (box-count) dimension in our fractal Liesegang systems (PbF_2 and PbI_2), and compare it with the fractal dimension obtained before (Table I).

In HarFA 5.5 software,[44] the image that needs to be analyzed should be transformed into black and white (BW image). A modified traditional box counting is used, where squares of the black and white regions are counted separately, those which cover the border of black object and those which just contain a white background (thus completely white). As a consequence of this modification, three fractal dimensions D_B, D_{BW}, and D_W are obtained, which are characteristic of the black plane, black-white border of black object, and white background, respectively. In case of our constructed Liesegang patterns, we are interested in the fractal dimension of the white region since the bands constitute the white part of our BW image. If we carry out such measurements for several sizes of square of the overlaid mesh, we can establish individual fractal dimensions as slopes of the plots of the functions N_B, N_{BW}, and N_W versus $\ln(1/r)$, according to the equations

$$N_B(r) = D_B\ln(1/r) + K_B, \tag{16}$$

$$N_{BW}(r) = D_{BW}\ln(1/r) + K_{BW}, \tag{17}$$

$$N_W(r) = D_W\ln(1/r) + K_W. \tag{18}$$

In order to obtain the Hausdorff dimension and the topological entropy, the fractal analysis of the HarFA software has been employed. The analysis was done on 11 bands taken as an arbitrary extract of the entire Liesegang pattern, using Mathematica software.[45] We constructed black and white images of geometrical patterns that resemble the experimental patterns prepared with the following concentrations for PbF_2: $[Pb^{2+}]$ = 0.250 M; $[F^-]=0.045$ M, and for PbI_2: $[Pb^{2+}]=0.250$ M; $[I^-]=0.045$ M. The Hausdorff dimensions were obtained as slopes of the function describing the white region in Eq. (15), and the values are recorded in Table I. The corresponding plots are depicted in Fig. 3.

It is seen that the values agree, to a great extent, with the analytical fractal dimensions ($D_{anal.}$) and the fractal dimensions obtained by the Benoît software ($D_{geom.}$), for the geometrical Liesegang patterns constructed by Mathematica. The topological entropy of the white regions (bands) in our

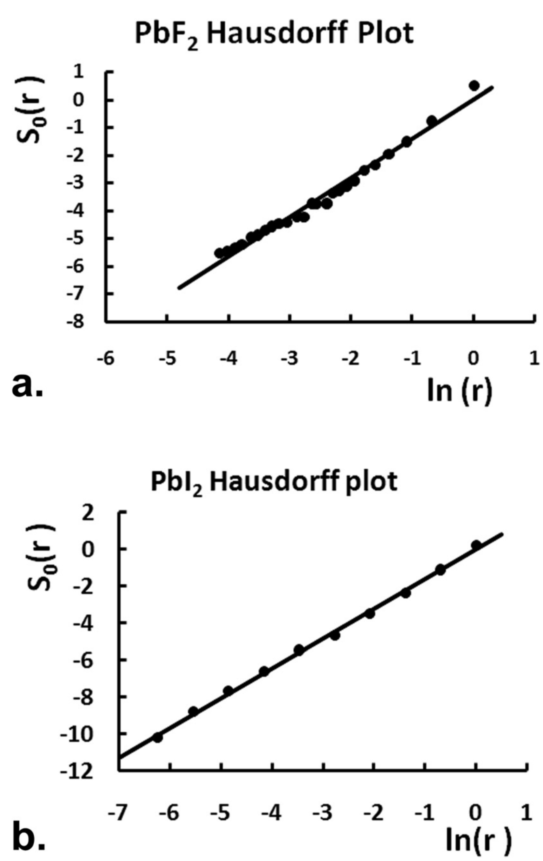

FIG. 3. HarFA plots of order zero for the geometrical Liesegang patterns of PbF_2 (a) and PbI_2 (b). The slopes yield the Hausdorff dimension (D_0). $D_0=1.410$ for PbF_2 and $D_0=1.613$ for PbI_2.

constructed Liesegang patterns was calculated from the Hausdorff dimension D_0 using the equation $S_0(r) = D_0 \ln r$ for each pattern, respectively, wherein the area of the entire image analyzed is 1127×181 pixels for the PbF_2 tube, and 1122×147 pixels for the PbI_2 tube. In order to compute the area or the size of the white region (white bands, S_w) of our Liesegang patterns, we use the relation[18]

$$S_w = \frac{K_W - K_{BW}}{K_B + K_W - K_{BW}}. \tag{19}$$

The size of the white bands of the PbF_2 geometrical Liesegang pattern obtained is $S_w = 0.06569$ using Eq. (19), and $S_w = 0.1190$ for the PbI_2 geometrical Liesegang pattern. To calculate the size in pixels, we multiply each fraction by the image area indicated above, which yields the actual region where fractal analysis is performed. For the PbF_2 pattern, the topological entropy is calculated as $S_0(r) = D_0 \ln r$, where $D_0 = 1.410$ and $r = 13400$, hence $S_0(r)$ of PbF_2 $= 13.39$. Similarly for the PbI_2 pattern, $S_0(r) = 15.94$, where $D_0 = 1.6129$ and $r = 19627$.[18] The D_0 values appear in Table I under the name $D_{Haus.}$

D. Information dimension and Shannon entropy ($q = 1$)

The Shannon entropy is a measure of the average information content when the random variable has an unknown value. Let n_{jk} be the frequency with which the fractal enters the j^{th} vel of size r_k in the k^{th} covering. We define the probability p_{jk} of the fractal within the j^{th} vel as the ratio of n_{jk} to the total number N_{Tk} of intersects of the fractal with all the vels (Eq. (21)), as follows:[46]

$$p_{jk} \stackrel{def}{=} \lim_{k\to\infty} \left(\frac{n_{jk}}{N_{Tk}} \right), \tag{20}$$

where

$$N_{Tk} \stackrel{def}{=} \sum_{j=1}^{N_k} n_{jk}. \tag{21}$$

For the k^{th} covering fractal, the probability (Eq. (20)) is rewritten as p_j, and the Shannon entropy is defined by[46]

$$S_1(r) = -\sum_{i=1}^{m} p_i \ln p_i. \tag{22}$$

The Shannon entropy (22) is defined for the order $q = 1$, and it depends on the probability and its logarithm, and on the number of events m with the probability $p_i > 0$. There is a linear dependence between the Shannon entropy and the information dimension (23), given by

$$S_1(r) = D_1 \ln r. \tag{23}$$

The information dimension, D_1, is a measure of the density of the fractal, determined from the relative frequency of occurrence of the fractal in each intersecting vel.[18] The information dimension D_1 also expresses how many real numbers are needed to specify a point in a fractal set; in other words, it counts the degrees of freedom for a point in a fractal set. Furthermore, the information dimension is used to determine how many bits of information are needed to specify a point to a given accuracy.[42] A lower D_1 indicates a greater density of the fractal characterized by greater clustering.[43]

We now attempt to calculate the Shannon entropies and the information dimensions for the same geometrical Liesegang patterns described above.

In order to obtain the information dimension and the Shannon entropy, the 2D *wavelet* analysis method of the HarFA software has been employed.[18] The Haar power spectrum transmission signals of a given topological pattern is transformed by a multi-revolution decomposition fast algorithm which utilizes the orthogonal wavelet bases.[47] Each signal is decomposed into components under different scales and this yields the wavelet transform of the pattern. In this analysis, a narrow peak (signal) is associated with low entropy, which embodies certainty and regularity; whereas a broad, flat peak expresses high complexity and uncertainty, and thus has a large spectrum entropy. Because the uncertainty of any event is associated with its states and probabilities, then the uncertainty of a signal correlates with a diffuse distribution and hence a blurred, broad peak.[47] The HarFA software selects an area (to be analyzed) of size $N \times N$, where N is an integer power of 2. Wavelet analysis is then performed by mapping the various datasets onto intensity values that are shades of grey, hue, red, green, or blue components of color information.[48]

The analysis was done on the 11 bands described above. The information dimensions were obtained as slopes of the function describing the white region (Eq. (16)). We found $D_1 = 1.517$ for the PbF_2 Liesegang pattern and $D_1 = 1.600$ for the PbI_2 Liesegang pattern. The dependence of Shannon entropy on the information dimension of the white region (bands) of the Liesegang patterns was calculated using the equation $S_1(r) = D_1 \ln r$ (Eq. (23)) for each pattern, respectively, with the area of the entire image analyzed equal to 1024×128 pixels. In order to compute the area or the size of the white region (S_w), we use Eq. (19).

The sizes of the white regions S_w are $S_w = 0.169$ for the PbF_2 pattern, and $S_w = 0.222$ for the PbI_2 pattern. These represent the fractions of the white regions (bands) of the two Liesegang patterns, respectively. For the size in pixels, we multiply each fraction, respectively, by the total area of analysis 128×128 pixels. Subsequently, the Shannon entropies calculated from $S_1(r) = D_1 \ln r$ are 12.03 for PbF_2, and 13.12 for PbI_2, respectively, with $r_{PbF_2} = 2769$ pixels, and $r_{PbI_2} = 3637$ pixels. The thermodynamic entropies are calculated from the extended Boltzmann formula

$$S = k_B\, S_1(r), \tag{24}$$

where k_B is the Boltzmann constant. All values are reported in Table II; and the corresponding plots are shown in Fig. 4.

Another interesting route for calculating the information dimension and the Shannon entropy is to take the frequency of occurrence of each band n_{jk}, as the area or size of each

TABLE II. Information dimension and Shannon entropy for PbF_2 and PbI_2 Liesegang patterns, obtained from the HarFA software and by the analytical method. The units of $S_{Boltz.}^{Har}$, $S_{Boltz.}^{anal.}$, and 3^{rd} law S are J mol^{-1}K^{-1}.

	D_1^{Har}	$S_1(r)^{Har}$	$S_{Boltz.}^{Har}$	3^{rd} law S (Ref. 49)	$D_1^{anal.}$	$S_1(r)^{anal.}$	$S_{Boltz.}^{anal.}$
PbF_2	1.517	12.03	100.02	110.5	1.361	12.07	100.3
PbI_2	1.600	13.12	109.08	174.9	1.387	13.45	111.8

band = width w_n multiplied by its height (namely the tube diameter), and the probability p_{jk} as the size ratio, as follows:

$$p_{jk} = \frac{size_{jk}}{size_{total}}; \quad \text{where } size_{total} = \sum_{j=1}^{N_k} size_{jk}. \tag{25}$$

Here N_k is obviously the total number of bands (11 bands) in the pattern. An important variant from Eq. (25) is introduced in our method to calculate the probability. Because the fractality of a Liesegang pattern depends on the topological distribution of the bands, it is imperative that the band location be implicated in the calculation of the fractal dimension and the entropy. Thus, the size of the k^{th} band in the j^{th} vel (Eq. (25)) is weighted (multiplied) by its location x_k. To maintain the dimensionless character of the probability, we weight the denominator by the total pattern length (ℓ) (spanning from upper edge of the first band to bottom edge of the last band). Thus, Eq. (25) is readjusted to

$$p_{jk} = \frac{size_{jk} \cdot x_k}{\ell \cdot size_{total}}; \quad \text{where } size_{total} = \sum_{j=1}^{N_k} size_{jk}. \tag{26}$$

Plots of individual Shannon entropy associated with each event m (the band in our pattern) versus $\ln size_k$ were constructed,[46] and the information dimension D_1 was thus calculated as the slope of each plot. The plots are displayed in Fig. 4, and exhibit a very good linearity. We found $D_1 = 1.361$ for PbF_2, and $D_1 = 1.387$ for PbI_2.

In this latter method, the size of the white bands (size$_{total}$ Eq. (25)) was 0.003936 for PbF_2 and 0.5000 for PbI_2 geometrical Liesegang pattern. So these are the fractions of the white regions (bands) of the two Liesegang patterns, respectively. To compare with the HarFA wavelet computation, we calculate the size in pixels as before. The corresponding Shannon entropies ($S_1(r) = D_1 \ln r$) were 12.07 for PbF_2 and 13.45 for PbI_2, with $r_{PbF_2} = 7098$ pixels, $r_{PbI_2} = 16240$ pixels. The thermodynamic entropies of the PbF_2 and PbI_2 are again calculated from the Boltzmann formula (24). The results are recorded in Table II; and the corresponding plots are highlighted in Fig. 5.

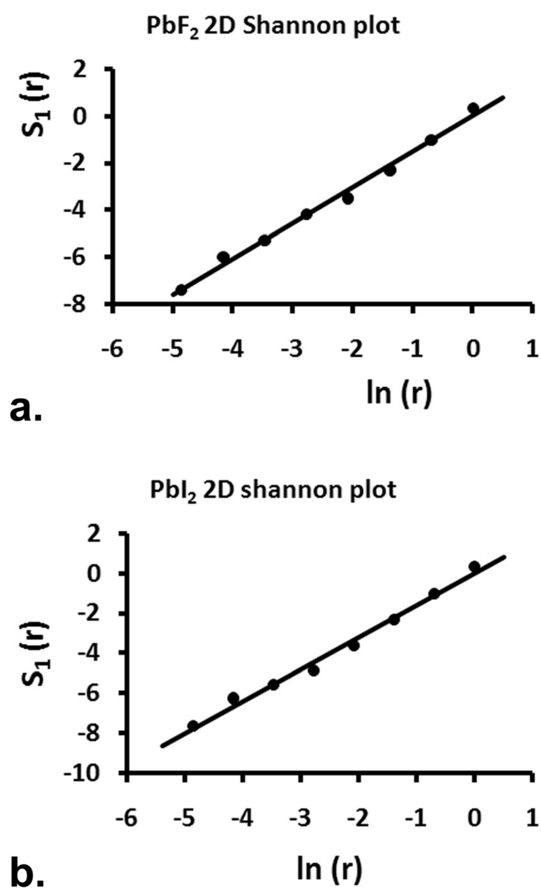

FIG. 4. HarFA plots of order 1, for the PbF_2 (a) and the PbI_2 (b) Liesegang patterns. The slopes of the straight lines yield the information dimension (D_1). $D_1 = 1.517$ for PbF_2 and $D_1 = 1.600$ for PbI_2.

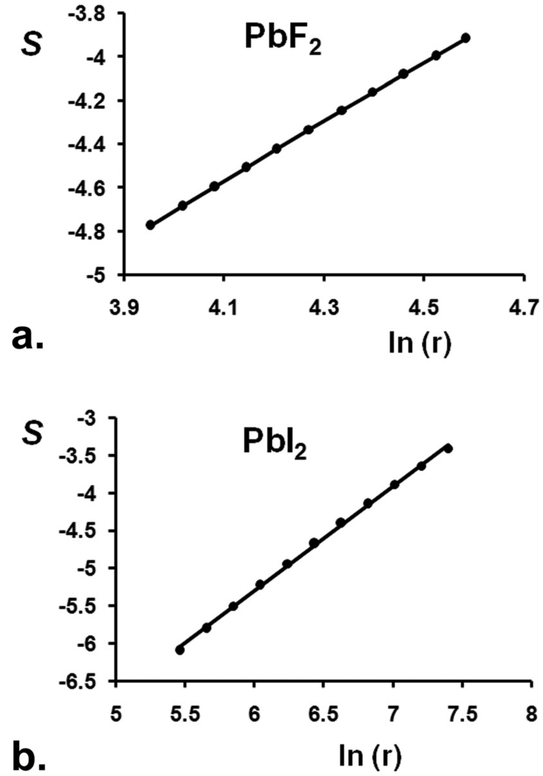

FIG. 5. Plots of S versus $\ln r$ for the geometrical Liesegang patterns of PbF_2 (a) and PbI_2 (b), obtained by the analytical method described in Sec. III D (second half). The slopes yield the analytical fractal dimension (D_1^{anal}). $D_1^{anal} = 1.361$ for PbF_2 and $D_1^{anal} = 1.387$ for PbI_2.

IV. CONCLUSIONS

The present study enabled the classification of the PbF_2 and PbI_2 Liesegang patterns as fractal structures that are characterized by their fractal dimensions. The fractal dimensions were calculated analytically, as well as by image analysis of both the experimental Liesegang patterns and the constructed geometrical Liesegang patterns that mimic them. The agreement between the analytical formulation of the geometrical fractals and the fractal dimension of real pattern images validates the classification of those patterns as fractal objects. An important comparison has also been drawn between the fractal dimension and the Hausdorff box count dimension obtained by the HarFA software. The values of the Hausdorff box counting dimension turned out to be close to the fractal dimension values (calculated before both analytically and by image analysis), as presented in Table I. Finally, in the zero-order regime, the topological entropies of the PbF_2 and PbI_2 patterns were estimated. The Shannon entropies and the information dimensions of constructed PbF_2 and PbI_2 Liesegang patterns, consisting of 11 bands each, with concentrations $[Pb^{2+}]_0 = 0.25$ M (for both), $[F^-]_0 = 0.045$ M, and $[I^-]_0 = 0.045$ M, have been computed. The computation of the Shannon entropies and information dimensions of the Liesegang patterns was carried out both mathematically and by the HarFA 2D wavelet method; and the values are reported in Table II. The numbers obtained by the two methods showed fairly good agreement. In addition, the thermodynamic entropies have been calculated for the PbF_2 and PbI_2 Liesegang patterns, by multiplying their Shannon entropy by Boltzmann's constant k_B. It was found that under the same initial conditions (both systems have equal concentrations of inner and diffusing (outer) electrolytes), the values are $S_{anal.}$ of $PbF_2 = 100.3$ J mol^{-1}K^{-1} and $S_{anal.}$ of $PbI_2 = 111.8$ J mol^{-1}K^{-1}, and S_{HarFA} of $PbF_2 = 100.02$ J mol^{-1}K^{-1} and S_{HarFA} of $PbI_2 = 109.08$ J mol^{-1}K^{-1}. In all calculations, PbF_2 turned out to be a more ordered Liesegang system than PbI_2. This appears to be in agreement with mere observation (see Fig. 1). Table II also lists the *Third Law* entropies of PbF_2 and PbI_2 (110.5 J mol^{-1}K^{-1} and 174.9 J mol^{-1}K^{-1}, respectively). Three important observations can be inferred from our calculations:

1. The fractal dimension and entropy values obtained through the different methods (routes) are in good agreement. This reveals the coherence of the treatment and the robustness of the various methods.
2. The similar orders of magnitude between the entropy values obtained and the Third Law entropies reported in the literature are promising, and reveal a good extent of reliability in the methods used.
3. The entropy values obtained for both PbF_2 and PbI_2 Liesegang patterns are lower than the reported entropies, exactly as expected. A pattern of Liesegang bands is more ordered than a homogeneous bulk of precipitate.

Entropy is an important measuring tool, not only because it gives the degree of disorder of a system in a given state, but because it contains the degree of uncertainty or complexity in a measured quantity, information, or signal. For instance, a low EEG entropy (reflecting enhanced EEG regularity and low brain complexity) has been associated with pathological states like sleep, anesthesia, schizophrenia, Parkinson's, and Alzheimer's diseases.[13] In cardiac systems, the higher the entropy value, the more the signal consists of random components of variability in heart beats.[12] It can be a good measure of the extent of arrhythmia or tachycardia. In Liesegang systems, like in geological landscapes consisting of banded textures,[9,10] entropy provides a good estimate of the dissipative nonequilibrium state of the pattern.

A more complete analysis is needed, wherein a bigger span of the spatial domain of the Liesegang pattern, and hence its time evolution should be considered. Further improvements include testing the calculations on other Liesegang systems (than PbF_2 and PbI_2). This gives a probe for the universality of the applied method.

ACKNOWLEDGMENTS

This project was supported by a University Research Board (URB) grant, American University of Beirut.

The authors thank Professor Oldrich Zmeskal of the Brno University of Technology for useful discussion and advice.

[1]R. F. Sultan, Acta. Mech. Sin. **27**, 119 (2011).
[2]R. E. Liesegang, Lieseg. Photograph. Arch. **37**, 305 (1896); **37**, 331 (1896).
[3]K. H. Stern, Chem. Rev. **54**, 79 (1954); K. H. Stern, *A Bibliography of Liesegang Rings*, 2nd ed. (Government Printing Office, Washington D.C., 1967).
[4]H. K. Henisch, *Crystals in Gels and Liesegang Rings* (Cambridge University Press, Cambridge, 1988).
[5]Wi. Ostwald, *Textbook of General Chemistry* (Verwandtschaftslehre, Engelmann, Leipzig, 1899),Vol. 2.
[6]Wi. Ostwald, *Lehrbuch der Allgemeinen Chemie, Teil: Verwandtschaftslehre, 2. Aufl.* (Engelmann, Leipzig, 1896–1902), Band 2, p. 778.
[7]I. M. Lifshitz and V. V. Slyozov, J. Phys. Chem. Solids **19**, 35 (1961).
[8]I. G. Main and F. H. Al-Kindy, Geophys. Res. Lett. **29**, 1121, doi:10.1029/2001GL014078 (2002).
[9]D. L. Anderson, "Plate tectonics as a far-from-equilibrium self-organized system," in *AGU Monograph: Plate Boundary Zone*, Geodynamics Series Vol 30, edited by S. Stein and J. Freymuller (American Geophysical Union, 2002).
[10]J. D. Phillips, Prog. Phys. Geogr. **19**, 309 (1995).
[11]I. Arzate-Vázqueza, J. J. Chanona-Péreza, G. Calderón-Domínguez, E. Terres-Rojas, V. Garibay-Febles, A. Martínez-Rivas, and G. F. Gutiérrez-López, Carbohydr. Polym. **87**, 289 (2012).
[12]T. T. Jartti, T. A. Kuusela, T. J. Kaila, K. U. O. Tahavanainen, and A. T. Välimäki, Br. J. Clin. Pharmacol. **45**, 277 (1998).
[13]C. Sitges, X. Bornas, J. Llabrés, M. Noguera, and P. Montoya, Int. J. Psychophysiol. **77**, 176 (2010).
[14]H.-J. Gdynia, H.-P. Müller, A. C. Ludolph, H. Köninger, and R. Huber, Eur. Jour. Neur. **16**, 1151 (2009).
[15]L. B. Rocha, R. L. Adam, N. J. Leite, K. Metze, and M. A. Rossi, Microsc. Res. Tech. **71**, 619 (2008).
[16]A. Y. Meigal and A. S. Voroshilov, Hum. Physiol. **37**, 855 (2011).
[17]P. Ball, *The Self-Made Tapestry: Pattern Formation in Nature* (Oxford University Press, Oxford, 1999).
[18]O. Zmeskal, P. Dzik, and M. Vesely, Comput. Math. Appl. **66**, 135 (2013).
[19]B. B. Mandelbrot, *The Fractal Geometry of Nature* (Freeman, San Francisco, 1982).
[20]F. C. Moon, *Chaotic and Fractal Dynamics: An Introduction for Applied Scientists and Engineers* (Wiley, New York,1992).
[21]T. Vicsek, *Fractal Growth Phenomena*, 2nd ed. (World Scientific, Singapore, 1992).
[22]É. Kápáti-Smidróczki, A. Büki, and M. Zrínyi, Colloid Polym. Sci. **273**, 857 (1995).
[23]A. Toramaru and A. Iochi, Forma **15**, 365 (2000).
[24]L. Mandalian and R. Sultan, Collect. Czech. Chem. Commun. **67**, 1729 (2002).

[25]M. Matsushita, M. Sano, Y. Hayakawa, H. Honjo, and Y. Sawada, Phys. Rev. Lett. **53**, 286 (1984).
[26]P. P. Trigueros, J. Claret, F. Mas, and F. Sagués, J. Electroanal. Chem. **312**, 219 (1991).
[27]P. Bak, Phys. Today **39**(12), 38 (1986).
[28]J. M. J. Fréchet and D. A. Tomalia, *Dendrimers and Other Dendritic Polymers* (Wiley, New York, 2002).
[29]F. Zaknoun, Th. Mokalled, A. Hariri, and R. Sultan, in *Precipitation Patterns in Reaction-Diffusion Systems*, edited by I. Lagzi (Research Signpost, Kerala, India, 2010), pp. 219–236.
[30]S. C. Müller, S. Kai, and J. Ross, J. Phys. Chem. **86**, 4078 (1982).
[31]T. Antal, M. Droz, J. Magnin, Z. Rácz, and M. Zrinyi, J. Chem. Phys. **109**, 9479 (1998).
[32]V. Nasreddine and R. Sultan, J. Phys. Chem. A **103**, 2934 (1999).
[33]C. K. Jablczynski, Bull. Soc. Chim. Fr. **11**, 1592 (1923).
[34]M. Droz, J. Magnin, and M. Zrinyi, J. Chem. Phys. **110**, 9618 (1999).
[35]R. Matalon and A. Packter, J. Colloid Sci. **10**, 46 (1955).
[36]P. Grassberger and I. Procaccia, Phys. Rev. A **28**, 2591 (1983).
[37]A. Rényi, *Probability Theory* (Elsevier B. V., Amsterdam, 1970).
[38]A. Garrido, Symmetry **3**, 487 (2011).
[39]*The Collected Papers of Lewis Fry Richardson*, Vol. 1: Meteorology and Numerical Analysis edited by L. F. Richardson, O. M. Ashford, H. Charnock, P. G. Drazin, J. C. R. Hunt, P. Smoker, and I. Sutherland (Cambridge University Press, Cambridge, 1993).
[40]B. B. Mandelbrot, "How long is the coast of Britain? statistical self-similarity and fractional dimension," Science **156**, 636 (1967).
[41]I. Zelinka, Ch. Guanrong, O. E. Rossler, V. Snasel, and A. Abraham, *Nostradamus 2013: Prediction, Model and Analysis* (AISC, 2013), Vol. 210, p. 455.
[42]J. J. Theiler, Opt. Soc. Am. A **7**, 1055 (1990).
[43]A. Giri, I. M. Choudhury, T. Dutta, and S. Tarafdar, Cryst. Growth Des. **13**, 341 (2013).
[44]O. Zmeskal, T. Bzatek, and M. Nezadal, *HarFA software*, version 5.5 (Brno University of Technology, Brno, 2004).
[45]S. Wolfram, *Mathematica software*, version 7 (Wolfram Research Inc., Hanborough, 2009).
[46]W. Kinser, Int. J. Cognit. Inf. Nat. Intell. **1**, 26 (2007).
[47]H. E. Zheng-you, Ch. Xiaoqing, and L. Guoming, *Proceedings of the International Conference on Power System Technology* (IEEE, 2006), pp. 1–6.
[48]See http://www.fch.vutbr.cz/lectures/imagesci/includes/harfa_introduction.inc.php for description of HarFA software.
[49]Chemical Rubber Company (CRC), *Handbook of Chemistry and Physics*, edited by D. R. Lide, CD rom version (CRC, Boca Raton, 2008).